Accurate Prediction of Protein NMR Spin Relaxation by Means of Polarizable Force Fields. Application to Strongly Anisotropic Rotational Diffusion

Moreno Marcellini, Minh-Ha Nguyen, Marie Martin, Maggy Hologne, Olivier Walker

THE JOURNAL OF PHYSICAL CHEMISTRY B

B: Biophysics; Physical Chemistry of Biological Systems and Biomolecules

Accurate Prediction of Protein NMR Spin Relaxation by Means of Polarizable Force Fields. Application to Strongly Anisotropic Rotational Diffusion

Moreno Marcellini, Minh-Ha Nguyen, Marie Martin, Maggy Hologne, and Olivier Walker

J. Phys. Chem. B, **Just Accepted Manuscript** • DOI: 10.1021/acs.jpcb.0c01922 • Publication Date (Web): 05 Jun 2020

Accurate Prediction of Protein NMR Spin Relaxation by Means of Polarizable Force Fields. Application to Strongly Anisotropic Rotational Diffusion

*Moreno Marcellini, Minh-Ha Nguyen, Marie Martin, Maggy Hologne and Olivier Walker**

Institut des Sciences Analytiques (ISA), Univ Lyon, CNRS, UMR5280, Université Claude Bernard Lyon1, Lyon France.

ABSTRACT

Among the various biophysical methods available to investigate protein dynamics, NMR present the ability to scrutinize protein motions on a broad range of time scales. ^{1}H-^{15}N NMR spin relaxation experiments can reveal the extent of protein motions across the ps-ns dynamics probed by the fundamental parameters ^{15}N-R_1, ^{15}N-R_2 and ^{1}H-^{15}N NOE that

can be well sampled by molecular dynamics simulations (MD). An accurate prediction of these parameters is subjected to a proper description of the rotational diffusion and anisotropy. Indeed, a strong rotational anisotropy has a profound effect on the various relaxation parameters and could be mistaken for conformational exchange. Although the principle of NMR spin relaxation predictions from MD is now well established, numerous NMR/MD comparisons have hitherto focused on proteins that show low to moderate anisotropy and make use of a scaling factor to remove artifacts arising from water model-dependence of the rotational diffusion. In the present work, we have used NMR to characterize the rotational diffusion of the α-helical STAM2-UIM domain by measuring the ^{15}N-R_1, ^{15}N-R_2 and ^{1}H-^{15}N NOE relaxation parameters. We therefore highlight the use of the polarizable AMOEBA FF and show that it improves the prediction of the rotational diffusion in the particular case of strong rotational anisotropy, which in turn enhances the prediction of the ^{15}N-R_1, ^{15}N-R_2 and ^{1}H-^{15}N NOE relaxation parameters without requirement to a scaling factor. Our findings suggest that the use of polarizable FFs could potentially enrich our understanding of protein dynamics in situations where charges

distribution or protein shape is remodeled over time like in the case of multidomain proteins or intrinsically disordered proteins.

INTRODUCTION

Biological processes and more particularly cell communication are achieved through interaction networks where protein dynamics is essential. Among the various biophysical techniques that allow to investigate protein dynamics, NMR is particularly attractive due to its capability to accurately explore structure and dynamics at atomic level. From this perspective, NMR may probe protein dynamics across ps-ms time scale. Faster ps-ns dynamics are obtained by measuring the most popular ^{15}N spin relaxation parameters such as longitudinal relaxation R_1, transverse relaxation R_2 and ^{1}H-^{15}N steady state heteronuclear NOE or ^{1}H-^{15}N DD/^{15}N CSA longitudinal or transverse cross correlation experiments while μs-ms slower motions could be captured by more specific CPMG and $R_{1\rho}$ relaxation dispersion.[1-2] These parameters characterize heavy atom-proton relaxation rates, probing both the local and global motion. Their analytical expression is based on a

linear combination of spectral densities *J(w)* operating at different frequencies and are the Fourier transforms of the heavy atom-proton vector autocorrelation functions *C(t).*[3-4] The most general level of analysis usually requires the characterization of spectral densities at five different frequencies but necessitates the measurement of extra NMR cross correlation terms.[5-6] Additionally, the use of the three main relaxation terms cited above, allows the calculation of reduced spectral densities[7] or quasi spectral density function[8] that does not necessitate any assumption of a particular motional model. An accurate description of these motions entails the use of well-established models that comprise the model-free formalism[9-10], closely related to the earlier two-step model[11] or another approach based on the slowly relaxing local structure (SRLS).[12] Due to recent unprecedented hardware and software improvement[13], the time scales probed by relaxation parameters have become accessible through the use of all-atoms molecular dynamics (MD) in a reasonable computational time. Thus, MD provides a direct method for cross-validation of force fields (FFs) by spin relaxation[14] or its prediction[15-19] and necessitates a correct determination of both the local NH bond motion (in case of a NH probe) and the global molecular tumbling represented by the corresponding $C_{loc}(t)$ and

$C_{global}(t)$ correlation functions respectively. It requires in turn a correct derivation of the rotational diffusion D_{rot} from the MD trajectory. To determine these parameters, one generally rely on fitting a sum of exponential functions to $C_{loc}(t)$ while the determination of D_{rot} is achieved through the use of different mathematical techniques[20-22] in the case of well-defined structured proteins. This parameter is more questionable in the case of intrinsically disordered proteins.[23-24] These considerations point to the importance of the accurate prediction of the overall tumbling (D_{rot}) but also the rotational anisotropy of this motion (D_{Δ}), since proteins that deviate from a spherical shape will tumble more rapidly about some directions than others. Additionally, stronger anisotropies can severely affect spin relaxation values.[25] Since the early work of Smith and Gunsteren about BPTI and Lysozyme[26], most of the recent studies that compare NMR spin relaxation and MD, involve proteins that have a low to moderate anisotropy ($1.0 < D_{\Delta} < 2.0$).[16,21,27] Whatever the methods used, the different bricks that constitute the relaxation parameters are constrained by the choice of a given force field (FF). From this perspective, the rotational diffusion has been proved to be difficult to evaluate and requires corrections to remove artifacts arising from force fields (FFs) and water model dependence. Most of the

corrections consist in using a scaling factor or a correction to the NH bond length to counterbalance the inaccuracy of water models.[20,28-30] From this point of view, we can separate the different FFs in two categories. In the most general case, biomolecular simulations are conducted by using empirical, fixed-charge FF, developed along with their corresponding water model.[31-32] FFs based on the popular AMBER and CHARMM families are well suited to model biological phenomena, but suffer from a lack of accuracy in determining rotational diffusion.[33] Moreover, an improved prediction of NMR spin relaxation would require the use of a zero-point vibration correction.[15] To account for a more accurate and realistic description of protein structure and dynamics, polarizable FF like Drude[34] or AMOEBA (Atomic Multipole Optimized Energetics for Biomolecular Application)[35] have been developed.[36] Several studies have demonstrated the benefits of treating biomolecular systems by including polarizability in peptide simulation.[37-38] While FFs are validated against NMR time averaged parameters like the general order parameter S^2, scalar couplings or residual dipolar couplings, less has been done to validate NMR spin relaxation parameters due to their intrinsic complexity. Thus, one may wonder if it possible to predict NMR spin relaxation parameters in a situation of (i) strong

rotational anisotropy and (ii) without turning to any scaling factor. To answer these questions, we have used the UIM domain of STAM2, a short 31 amino acids α-helical peptide that is characterized by a strong rotational anisotropy. In an effort to predict the ^{15}N R_1, ^{15}N R_2 and ^{1}H-^{15}N NOEs NMR relaxation parameters, we have used four different FF, comprising the polarizable AMOEBA FF and three other non-polarizable FF: the ff99SB-disp[39], ff15ipq[40] and C36m.[41] As a first approach, we have replaced the MD calculated rotational diffusion by its experimentally derived counterpart to circumvent the problem of the rotational diffusion evaluation and water model. As a second approach, we have used the rotational diffusion derived from the MD trajectories. Whatever the approach, we show that the use of a polarizable FF significantly improves the prediction of the different relaxation parameters without the need of a scaling factor while the ff15ipq associated to the SPC/E_b water model gives the best predictions among the non-polarizable FFs.

EXPERIMENTAL METHODS AND THEORY

Protein production. The human STAM2 UIM construct was designed in pETM60 plasmid with NusA and 6-His tag fused to the N-terminus under the regulation of a lac operon and has been purchased from Genecust. The plasmid was then transformed into E. coli BL21 GOLD (Millipore). Cells were grown in M9 medium supplemented with 1 mM $MgSO_4$, 1 mM $CaCl_2$, 6 mg/L thiamine, 1% (v/v) trace element solution [5 g/L EDTA, 0.5 g/L $FeCl_3.6H_2O$, 5 mg/L ZnO, 1 mg/L $CuCl_2.2H_2O$, 1 mg/L $Co(NO_3)_2.6H_2O$, and 1 mg/L $(NH_4)_6Mo_7O_{24}.4H_2O$], 50 mg/L kanamycin and 1 g/L $^{15}NH_4Cl$ as sole nitrogen source for a uniform ^{15}N labelling and 2.5 g/L of $^{12}C_6$-D-Glucose. The cells culture was grown at 37 °C to an A600 of 0.6-0.8 and the overexpression is induced by adding 1 mM IPTG. After 5 h of induction at 30 °C, cells were lysed in 50 mM Tris buffer, 250 mM NaCl, 10 mM imidazole, 0.04 %(v/v) β-mercapto-ethanol, 5 %(v/v) glycerol and 1 tablet of Complete® protease inhibitors from ROCHE. The clarified cells lysate was loaded on a Ni-NTA Fast Flow column (GE Healthcare) equilibrated with 50 mM Tris-HCl (pH 7.8), 250 mM NaCl, 10 mM imidazole, 1%(v/v) glycerol and 0.04%(v/v) β-mercaptoethanol. The bound protein was eluted with a 10-400 mM imidazole gradient. NusA and His6 tag were cleaved by TEV protease at 4 °C O/N and discarded by a second Ni-NTA column. UIM was then

purified by a Superdex 75 gel filtration column (GE Heathcare) equilibrated in 20 mM sodium phosphate buffer (pH 6.8) and 130 mM NaCl. The elution peak was desalted and concentrated in a Microcon concentrator tube with 2 kD cut-off.

NMR experiments and processing. NMR spin relaxation measurements were carried out at a proton frequency of 600 MHz at 288 K on a Bruker Avance III HD equipped with a triple HCN probe. Relaxation measurements including ^{15}N longitudinal (R_1), transverse (R_2) relaxation as well as the ^{1}H-^{15}N heteronuclear cross-relaxation rates were performed using the previously published method[42]. Prior to any experiments, the temperature was calibrated with a methanol-d_4 sample. NMR spectra were recorded with spectral widths of 2189 Hz in the ^{15}N dimension and 11160 Hz in the ^{1}H dimension. For the R_1 experiments, we have used ten relaxation delays ranging from 40 to 2400 ms with a recycling delay of 4 s. The delays are the following: 40, 200, 400 (twice), 600, 800, 1100, 1400 (twice), 1700, 2200 and 2400 ms. In the case of R_2 experiments, we have used 13 relaxation delays ranging from 8 to 448 ms with a recycling delay of 4 s. The delays are the following: 8, 32, 64, 96 (twice), 160, 192 (twice), 224, 256, 304, 352, 384, 416 and 448 ms.

For heteronuclear NOE experiments, 2D spectra were recorded with and without presaturation of amide protons and a recycling delay of 4.5 s. Longitudinal and transverse relaxation parameters were estimated by fitting the measured peak intensities to a single exponential decay, using a two-parameter fit. The uncertainty of the relaxation parameters was estimated by Monte-Carlo simulation of the fitted parameters as implemented in the Relaxfit program.[42]

NMR spin relaxation simulations as a function of rotational anisotropy. To model the effect of an increasing rotational anisotropy on the R_1, R_2 and NOE parameters we have used the standard equations expressed as a linear combination of spectral densities:[4]

$$R_1 = 3(d^2 + c^2)J(\omega_N) + d^2[J(\omega_H - \omega_N) + 6J(\omega_H + \omega_N)] \quad (1)$$

$$R_2 = \frac{1}{2}(d^2 + c^2)[4J(0) + 3J(\omega_N)] + \frac{1}{2}d^2[J(\omega_H - \omega_N) + 6J(\omega_H) + 6J(\omega_H + \omega_N)] + R_{ex} \quad (2)$$

$$NOE = 1 - \left|\frac{\gamma_H}{\gamma_N}\right| d^2 \frac{[6J(\omega_H + \omega_N) - J(\omega_H - \omega_N)]}{R_1} \quad (3)$$

Where $d = -\frac{\mu_0}{4\pi} \times \frac{\gamma_H \gamma_N}{4\pi r_{HN}^3}$ is the strength of the ^{1}H-^{15}N dipolar coupling, $c = -\frac{\omega_N \times CSA}{3}$, ω_H and ω_N are the resonance frequencies of ^{1}H and ^{15}N respectively, CSA is the anisotropy of the ^{15}N chemical shift tensor, assumed axially symmetric, γ_H and γ_N are the gyromagnetic ratios of the nuclei, h is Plank's constant and R_{ex} is the conformational exchange contribution (if any) to the measured R_2. These equations provide the basis for extracting information on protein dynamics from NMR relaxation measurements. To translate into a physical picture of protein dynamics, the spectral densities $J(\omega)$ are expressed as a combination of local and global reorientation, assuming there is no correlation between the local dynamics and the global molecular tumbling, one can define a global correlation function $C(t)$:

$$C(t) = C_{global}(t) \times C_{local}(t) \quad (4)$$

Although extended models exist, we have chosen to use the standard model-free approach[9-10] to represent $C_{local}(t)$:

$$C_{local}(t) = S^2 + (1 - S^2) \times exp\left(-t/\tau_{loc}\right) \quad (5)$$

where τ_{loc} represents the correlation time of a bond motion and S^2 stands for the order parameter that represents the dimensionless averaged amplitude of the bond motion. In the case of an axially symmetric diffusion tensor, the global $J(\omega)$ can be rewritten as[43]:

$$J(\omega) = \frac{2}{5}\sum_{i=1}^{3} \frac{A_i^{ax} D_i^{ax}}{\left(D_i^{ax}\right)^2 + \omega^2} \qquad (6)$$

with

$$D_1^{ax} = (5D_{\perp} + D_{\parallel}); \qquad D_2^{ax} = (2D_{\perp} + 4D_{\parallel}); \; D_3^{ax} = 6D_{\perp}$$

and $A_1^{ax} = 3z_d^2(1 - z_d^2)$; $A_2^{ax} = \frac{3}{4}(1 - z_d^2)^2$; $A_1^{ax} = \frac{1}{4}(3z_d^2 - 1)$

where $D_{\parallel}$ and $D_{\perp}$ stand for the principal components of the axially symmetric tensor. z_d denotes the z coordinates of a NH unit vector in the principal axis frame of the diffusion tensor and is related to the molecular axis frame following the general transformation:

$$\begin{bmatrix} x_d \\ y_d \\ z_d \end{bmatrix} = R(\alpha,\beta,\gamma) \begin{bmatrix} x \\ y \\ z \end{bmatrix} \qquad (7)$$

R being the passive rotation matrix defined by its Euler angles according to the *zyz* convention in 3D space.[44] For a complete description in the case of a fully anisotropic rotational diffusion tensor, one can refer to previous papers for the analytical expression of the relaxation parameters.[43,45-46]

Rotational diffusion analysis. The rotational diffusion tensor of the protein was derived from the orientation dependence of the ρ factor described previously.[47] The ρ factor is expressed as $\left(\frac{2R_2'}{R_1'} - 1\right)^{-1}$ where R_2' and R_1' correspond to the transverse and longitudinal relaxation rates modified to subtract the contributions from high-frequency motions.[48] The advantage of using this ratio instead of the individual values of these parameters is that it is independent, to a first approximation, of the site-specific variations in the strength of ^1H-^{15}N dipolar coupling and ^{15}N chemical-shift anisotropy. Moreover, in the case of protein core residues, the R_2'/R_1' ratio primarily depends on the overall tumbling and is practically insensitive to fast, subnanosecond backbone dynamics.

Structure of the UIM domain. The three-dimensional structure of the UIM domain alone was obtained by homology modeling. As already demonstrated in earlier studies, the amino acid sequences of STAM2-UIM and Vps27-UIM1 share 55% identity and 70% similarity. Moreover, NMR has demonstrated that the STAM2 UIM domain adopts a α-

helical structure in solution[49] from residue E170 to residue E184 (currently renumbered E10 to E24 for simplicity in the current study, see supporting information). We used the UIM1 domain[50] of Vps27 (PDB code 1Q0V) as a template to model the structure of the UIM domain by means of the Modeler program.[51]

MD simulation. Molecular Dynamics (MD) simulations were carried out on GPUs by means of GROMACS 5.1.4[52], software with the CHARMM36m and AMBER ff99SB-disp force fields, or using ACEMD[53] software with AMBER ff15ipq and finally using Tinker and OpenMM[54-55] software with AMOEBA force field. For all cases, temperature and pressure were set to 300 K and 1.013 bar. All simulations include explicit solvent and H-bonds constrained to the length defined in the force field. MD analysis were performed with GROMACS software, a forked version of PLUMED (to compute quaternions)[20] and the SpinRelax[15] program.

GROMACS simulations. The protein was set in a dodecahedron water box with a minimum distance between the protein and the side equal to 1.2 nm. Counter ions (Na^+

and Cl^-) were added to adjust the net charge to zero (C_{NaCl} = 0.15 M). Equilibration involves the removal of isolated intruding water molecules. 2500 steps energy minimization followed by a gradual relaxation of side-chain and backbone restraints over 2 ns was conducted from 5000 to 0 kJ mol^{-1} nm^{-2}. Temperature and pressure were coupled with V-Rescale thermostat[56] and Berendsen's barostat.[57] Electrostatic interactions were handled by Particle Mesh Ewald (PME) methods[58] and van der Waals potential was treated by simple cutoff of 1.2 nm. Constraints of all bonds to the length defined by the FF were processed by LINCS algorithm.[59] The SETTLE algorithm[60] was used to constrain the rigid water molecule model. The final structure obtained after equilibration was retained as the starting configuration for 20 quasi-independent simulations. Each trajectory has been recorded every 5 ps for analysis and the integration time step was set to 2 fs. The trajectory length was set to 50 ns. For each simulation, the velocities of the particle were generated at start-up yielding a family of 20 different trajectories.

ACEMD simulations. The protein was set in a cubic box by applying 1.2 nm buffer to the protein coordinates, filled with water molecules and the specific counter-ions as in the previous case. Energy minimization was run for 1000 steps, followed by NVT equilibration for 200 ps with time-step of 2 fs and concluded with NPT equilibration in two steps: first with constraints during 1 ns and secondly without constraints for 1 ns. We used a Langevin's thermostat with dumping of 1 ps and Berendsen's barostat with pressure relaxation time of 800 ps. The Coulomb's electrostatic was described by PME (Particle Mesh Ewald) method with cutoff at 0.9 nm and grid-spacing of 0.1 nm, whereas the van der Waals forces were described by a switching function with a cutoff at 0.75 nm. The 50 ns runs were carried out in NVT ensemble. For this specific case, we have produced 20 quasi-independent trajectories, by generating new sets of velocity at start-up, giving rise to a total trajectory of 1μs.

Tinker and OpenMM simulations. The latest version of TINKER has OpenMP shared-memory parallelization of AMOEBA simulations, while OpenMM[61] is accelerated for GPU-based calculations. The generation of protein, water and counter-ions in a cubic box was

made by using GROMACS tools, adding a buffer of 1 nm to the protein (due to the computational intensity of the mechanic of the force field, to obtain a reasonable simulation speed, we needed to reduce the number of water molecules). We used the latest version of the AMOEBA force field[62]. The energy minimization was run through MINIMIZE. NVT and NPT equilibrations were run via DYNAMIC. In NVT equilibration (50 ps) the trajectory was integrated via RESPA integrator with a time step of 2 fs, whereas the NPT (100 ps) trajectory was integrated via VERLET integrator with a time step of 1 fs. In all cases, the HEAVY-HYDROGEN keyword was set so that we could use longer time-steps (Tinker manual suggests time-step below 1 fs with no mass-repartition, up to 3 fs can be used with RESPA integrator and heavy-hydrogen). Dipole convergence criterion was set POLAR-EPS = 0.001 D, and the polarization was computed by perturbation theory at the third order (POLARIZATION = OPT3).[63] Temperature and pressure were coupled with Bussi thermostat and Montecarlo barostat. During thermalization and density equilibration, the atomic distances of the heavy atom-hydrogen bonds were restrained by applying the RATTLE algorithm (water was never restrained because the system becomes computationally intractable). Production run were integrated via RESPA

integrator with a time-step of 2 fs, keeping same condition for barostat and thermostat. Conversion from Tinker .arc file to GROMACS .xtc file format was carried out by awk and Python scripts. In this current case, we performed 10 independent equilibrations. The simulation velocity in a GeForce GTX 980 is approximately ~ 5 ns/day, whereas in GeForce GTX 780 Ti is ~ 3 ns/day, and in a Tesla P100 at CINES is ~ 7 ns/day.

RESULTS AND DISCUSSION

The effect of rotational anisotropy on NMR spin relaxation

To account for the effect of an increasing rotational anisotropy on NMR spin relaxation data, we have used the analytical expression presented in the theory section above. The determination of the dynamical properties of a molecule by NMR relies on its shape. While an ideal sphere tumbles isotropically in solution so that all orientations within a molecule are equivalent, any deviation of this case will result in an anisotropy of its overall rotational diffusion in solution, which could be the case for an elongated rod, multidomain proteins or intrinsically disordered proteins. This, in turn, will lead to an orientational dependence of the various processes of nuclear spin relaxation that are modulated by molecular

motions. Orientational dependence is probed by ^{1}H-^{15}N bond vectors in our case and appears as a difference in the apparent tumbling rate. If we assume a molecule with its three principal components of the overall diffusion tensor D_x, D_y, D_z with $D_z > D_y > D_x$, an axial rotational tumbling will reduce to two components with $D_z \equiv D_{||}$ and $D_y = D_x \equiv D_{\perp}$. For a NH vector parallel to the || axis, its reorientations will be caused by molecular rotations around the $\perp$ axis so that the apparent rotational diffusion rate for this vector will be determined by $D_{\perp}$. Conversely, reorientation of a vector perpendicular to the || axis will be affected by $D_{||}$ and thus will proceed faster. These differences in molecular tumbling rates and internuclear vector orientations will lead to different modulation of the relaxation parameters and will increase with the rotational anisotropy. Moreover, this effect has to be accurately treated as it could be mistaken for conformational exchange.[25]

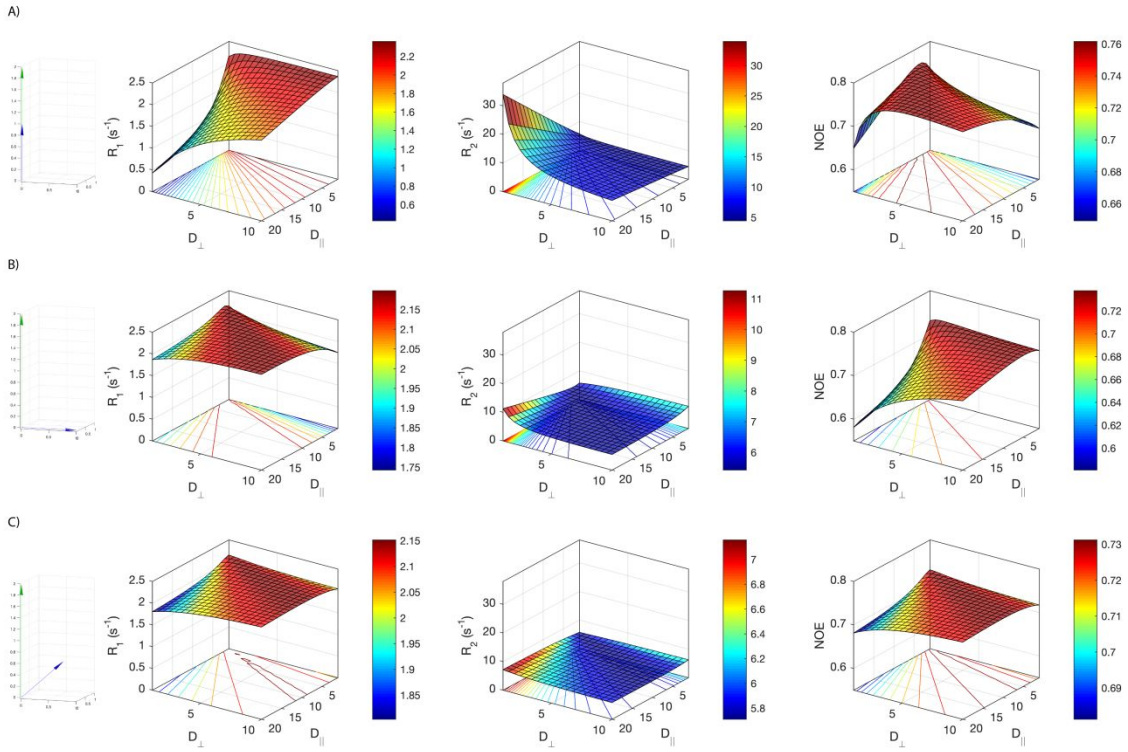

Figure 1. Dependence of the NMR spin relaxation parameters R_1, R_2 and NOE as a function of various degrees of anisotropy ($D_\Delta = D_{||} / D_\perp$) and NH vector orientation with respect to the principal axis frame (PAF). On the left panel, the $D_{||}$ axis of the PAF is represented in green along the z axis of the laboratory frame and three NH unit vectors are presented with a 0° (A), 90° (B) and 54° (C) orientation with respect to the $D_{||}$ axis of the PAF. The synthetic data were obtained by assuming local model-free combined with an axially symmetric molecular reorientation (see analytical expressions in experimental

methods). Typical parameters for restricted local backbone dynamics in protein core were used with S^2 = 0.84, a local motion τ_{loc} = 20 ps, a global tumbling τ_c = 4.0 ns for a ^{1}H frequency of 600MHz. Plain lines represent the surface projection for a given anisotropy.

For a complete description of the theoretical expressions describing these motions, we refer the reader to the previous work of Woessner.[64] To account for this theoretical framework, we have simulated the three relaxation parameters R_1, R_2 and NOE in the case of an axially symmetric model (see experimental methods for a description of the analytical expression used here) in the case of three distinct orientations of a NH bond vector. Figure 1 shows the results obtained for three different orientations of a NH vector with respect to the principal axis frame (PAF). For a given set of dynamical parameters that corresponds to a protein of ca ~8kDa (τ_c = 4.0 ns, τ_{loc} = 20 ps, S^2 = 0.84), there is a significant difference for the three relaxation parameters as a function of bond vector orientation and rotational anisotropy. For a rather low anisotropy (~1-2), the orientation of a NH vector has practically no effect on the relaxation parameters. For a bond vector that would lie parallel to the long axis of the PAF ($D_{||}$) and a significant increase of the

anisotropy (D_Δ ~ 4 to 10), one observes a profound modification of each relaxation parameters. Conversely, for a NH vector orientation that would lie 90° or 54° away from the $D_{||}$, a change of the anisotropy has a weak or moderate effect on any of the relaxation parameters. Increasing the rate of the local motion to 200 ps significantly affects the values of NOE while it has practically no effect on R_1 or R_2 (see figure S1A). Finally, if one considers the case of a NH vector that undergoes a significant flexibility (S^2 = 0.2 and τ_{loc} = 200 ps), R_1 and R_2 are less affected by the rotational anisotropy while NOEs significantly drop and are influenced in the case of a NH vector lying along the $D_{||}$ axis (Figure S1B).

Rotational diffusion of the UIM domain

Having shown that rotational anisotropy is a crucial parameter in the determination of the spin relaxation values, we have determined the rotational diffusion parameters from NMR relaxation data recorded for the UIM domain of the STAM2 protein. The UIM domain contains 31 amino acids that fold into an α-helix between E10 and E24 while the rest of this domain remains flexible (see supporting information).[65] We have used the ρ

factor method[66-67] for its ability to be valid for higher anisotropies (see experimental methods)[47]. Table 1 presents the results obtained for an isotropic and an axially symmetric model. In the case of an axially symmetric tensor, we have fitted 4 parameters, the two principal values of the rotational diffusion tensor along with the two angles that define the position of the PAF with respect to the laboratory frame. Since two of the eigenvalues are equal in the case of the axially symmetric model, the orientation of the diffusion tensor can be described by the orientation of the unique eigenvalue $D_{||}$. Therefore, we can express this orientation using only α and β angles and set $\gamma = 0$. It has to be recalled that the relaxation parameters are not sensitive to the directionality (sign) of the NH-vector coordinates.[66] Figure S2 shows the orientation of the unique axis of the rotational diffusion tensor that is roughly aligned along the α-helical motif of the UIM domain. Each of the NH bond vector orientations are defined with respect to the PAF. Only residues that belong to the well-defined α-helical region of UIM and that do not show any conformational exchange (A15 and L20 excluded) have been used for the analysis. As can be seen in Table 1, the axially symmetric model agrees with the experimental data significantly better than the isotropic model: the F-statistics analysis of the fit results in the

probability P = 5.3 × 10^{-10} that this could occur by chance. The use of a more complicated, fully anisotropic model, did not improve the fitting procedure and is not presented here.

Table 1. Rotational diffusion tensor parameters for UIM derived from ^{15}N relaxation data using an isotropic or axially symmetric model of the overall tumbling.

Model	D_x[a] (≡ $D_\perp$)	D_y[a] (≡ $D_\perp$)	D_z[a] (≡$D_{\|\|}$)	α[b]	β[b]	γ[b]	τ_c[c]	Anisotropy[d]	χ^2/df[e]	P[f]
Isotropic	4.55 (0.07)	4.55 (0.07)	4.55 (0.07)	-	-	-	3.66 (0.06)		8.0	
Axially-symmetric	2.2 (0.3)	2.2 (0.3)	11.7 (0.9)	120 (22)	57 (16)	-	3.10 (0.58)	5.3 (1.1)	1.4	5.3 × 10^{-10}

[a] Principal values (in 10^7 s^{-1}) of the rotational diffusion tensor, ordered so that $D_x \le D_y \le D_z$. In the case of an axially symmetric model, $D_z \equiv D_{||}$ and $D_y = D_x \equiv D_\perp$.

[b] Euler angles {α, β, γ} (in degrees) describe the orientation of the principal axes frame of the rotational diffusion tensor with respect to protein coordinate frame. Proper Euler angles have been defined with successive rotation around z(α)y(β)z(γ). In the case of an axially symmetric model, $\gamma = 0$.

[c] Overall rotational correlation time (in ns) of the molecule, $\tau_c = \frac{1}{[2\,Tr(\underline{D})]}$

[d] The degree of anisotropy of the diffusion tensor, $D_\Delta = 2D_z / (D_x+D_y)$ or $D_{||} / D_\perp$ in the case of an axially symmetric model.

[e] Residuals of the fit divided by the number of degrees of freedom

[f] Probability that the reduction in χ^2 (compared to the isotropic model) could occur by chance. The axially symmetric model gives a statistically much better fit than the isotropic model.

Using the experimental rotational diffusion to predict relaxation parameters

That UIM is affected by a significant anisotropy has encouraged us to compare different FFs for their ability to predict rotational diffusion and relaxation parameters. While computing D_{rot} by means of non-polarizable FFs could give rise to overestimated values, we were seeking to understand if the additional physics found in the AMOEBA polarizable FF allows a more accurate prediction of the standard spin relaxation parameters, i.e ^{15}N-R_1, R_2 and ^{1}H-^{15}N heteronuclear NOEs. To address this question, we have performed MD simulations of the short UIM helical domain. As a sake of comparison, we have used different FFs of the AMBER (ff99SB-disp[39] and ff15ipq[40]) and CHARMM family (C36m).[41] All simulations were run in explicit water (see experimental methods). While FFs were developed and improved with their respective water-models, we have used the SPC/E_b and AMOEBA water models associated with the ff15ipq and AMOEBA FFs respectively.

The SPC/E_b water model has been developed from the original SPC/E model with a slight increase in the O-H bond. It has been successfully tested and validated on four globular proteins (ubiquitin, protein G, barstar and BPTI) that exhibit a weak rotational anisotropy.[29] We have used the TIP3P-Charmm and a99SB-disp water models along with the respective Charmm36m and ff99SB-disp FFs. The specific TIP3P-Charmm water model is a TIP3P modified in the dispersion coefficient of the LJ interaction[41] while the a99SB-disp is based on the original TIP4P-D water model and has introduced small changes in the water vdW interaction terms.[39] All simulations have been run with a total trajectory duration of 1μs divided into 20 replicas of 50 ns. Indeed, it has been demonstrated that the simulations issued from several replicas are more reliable compared to a single, long simulation.[68] This duration is in agreement with 1-2 orders of magnitude above the expected tumbling time recommended previously[69] and ensures a sufficient conformational sampling for the estimation of the different relaxation parameters. Furthermore, the UIM domain keeps its α-helical fold for the majority of the simulations and FFs (Figure S3). The calculation of the relaxation parameters has been carried out by analyzing the MD trajectories following our well established protocol.[15,20]

Here we have compared two different methods to predict the relaxation parameters. First and foremost, we have chosen to introduce the values of D_{iso} and D_{Δ} that were derived from the NMR analysis. In this way, we avoid the problem of both the water-model[33] and the finite-size effects of the simulation box.[70-71] Secondly, we have used the MD-predicted D_{iso} and D_{Δ}. For the first method, D_{rot} has been extracted from NMR spin relaxation experiments (see Table 1).

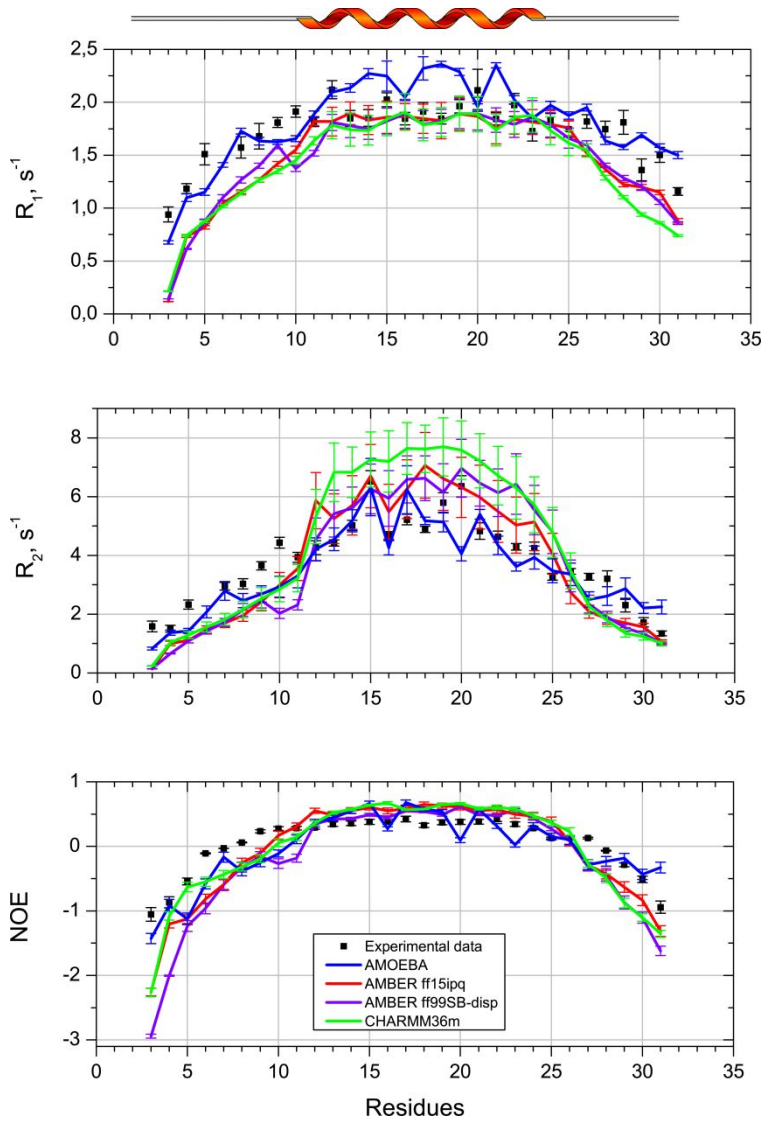

Figure 2. Experimental (black symbols) and computed NMR spin relaxation parameters (solid lines) ^{15}N R_1, ^{15}N R_2 and ^{1}H-^{15}N NOE for the different FFs used in this study. The global rotational diffusion D_{iso} and rotational anisotropy D_{Δ} are fixed by the experiment while the zero order correction parameter ζ has been fixed to 0.89.[72] The UIM secondary structure is represented at the top of the relaxation parameters.

The use of an axially symmetric model is also confirmed by MD and the values of the average radii of gyration obtained by the four FFs (see Table S1). The axial components of the diffusion tensor $D_{||}$ and $D_{\perp}$ (Table 1) were experimentally derived by considering the residues of the well folded helical region and that do not show any conformational exchange (A15 and L20 excluded). As a matter of consistency, the computation of the internal correlation function from MD simulations was conducted by selecting similar residues and using the following expression: $D_{\Delta} = D_{||} / D_{\perp}$ and $D_{iso} = 1/3.(D_{||} / D_{\Delta}).(2 + D_{\Delta})$.[73] No further optimization of parameters such as D_{iso}, D_{Δ}, CSA and ξ has been introduced in the analysis, ξ being the correction constant that describes the zero-point vibration of the N-H bonds.[72]

To account for the goodness of the predicted relaxation parameters compared to the experimental ones, we defined the χ^2 parameter:

$$\chi^2 = \sum_k \sum_{j=1}^{n} \left(\frac{O_j - P_j}{\sigma_k} \right)^2 \quad (8)$$

Where O_j is the experimentally observed value for the residue j and P_j is the corresponding predicted value derived from the analysis of the MD simulation, $k \in$ (R_1, R_2, NOE) and σ_k is the standard deviation of the corresponding relaxation parameter.

Table 2. Values of χ^2 indicating the goodness of the predicted R_1, R_2 and NOE for the different FFs and water-models used in this study.

Force Field (water model)	$\chi^2 (D_{iso}, D_{\Delta})^{exp}$	$\chi^2 (D_{iso}, D_{\Delta})^{MD}$
ff99SB-disp (TIP4P-disp)	60.9	105.3
ff15ipq (SPC/E_b)	41.2	71.7
C36m (TIP3P-charmm)	71.1	131.7
AMOEBA (AMOEBA)	23.3	22.6

$(D_{iso}, D_{\Delta})^{exp}$: spin relaxation parameters are predicted according to the experimental rotational diffusion and anisotropy. $(D_{iso}, D_{\Delta})^{MD}$: spin relaxation parameters are predicted according to the calculated rotational diffusion and anisotropy derived from MD simulations.

As can be seen in Figure 2 and Table 2, the agreement between experimental and predicted relaxation data depends on the considered FF. While polarized and empirical FFs show roughly the same agreement with respect to the NOE data, they exhibit a profound difference in the prediction of longitudinal and transverse relaxation rates. Non-polarizable FFs underestimate R_1 while the AMOEBA FF displays a good match with the

experimental R_1 all along the UIM sequence. In the case of R_2 that shows a significant increase in the helical part of UIM, non-polarizable FFs overestimate R_2 in this region while they underestimate R_2 in the flexible N- and C-terminus part of UIM. Moreover, the gap between the maximum and the minimum values predicted for R_2 is larger when a non-polarizable FF is used.

Our data clearly evidence that the use of the polarizable AMOEBA FF improves the prediction of NMR spin relaxation parameters compared to empirical FFs in the particular case of an elongated rod. To understand this discrepancy, we have to pinpoint the most important parameters responsible for these differences. As illustrated by Figure S4, we can notice a clear contrast in the decay of the correlation functions associated with some selected residues K7, I14, Q25 or Q28 located in different regions of UIM, which in turn induces a significant difference in the internal correlation function $C_I(t)$ as seen in Figure S5. Consequently, our observations suggest that the AMOEBA polarizable FF allows to grasp a more intricated motional network.

The AMOEBA FF accurately predicts D_{rot}

Thusly, as a second method, we have investigated the ability of the different FFs to predict the rotational diffusion of UIM. The isotropic value of the rotational diffusion D_{iso} is an essential parameter that remains a staple in the determination of relaxation rates. It contributes to the global tumbling of the correlation function through its axial components $D_{||}$ and $D_{\perp}$.[15] The calculated values of $D_{||}$, that represents the axis of fast overall rotation, span a large range from 8.79×10^7 to 36.60×10^7 s^{-1} with respect to the used FFs (see Table 3).

Table 3. Characterization of the rotational diffusion tensor of the UIM domain for the different FFs used in this study

	Exp	ff99SB-disp	ff15ipq	C36m	AMOEBA
$D_{||}$[a]	11.70 (0.90)	31.70 (3.50)	17.40 (2.30)	36.60 (5.10)	8.79 (0.60)
$D_{\perp}$[a]	2.20 (0.30)	1.53 (0.20)	4.13 (0.50)	5.83 (0.80)	2.28 (0.20)
D_{Δ}	5.30 (1.10)	20.80 (2.30)	4.21 (0.50)	6.29 (0.90)	3.86 (0.30)
D_{iso}[a]	5.40 (0.50)	11.60 (1.30)	8.55 (1.10)	16.10 (2.30)	4.45 (0.30)

[a]Values are given in 10^7 s^{-1}. Errors are specified into parentheses.

This is not surprising as D_{iso} from MD simulations is known to be overestimated due to the low viscosity of water models (TIP3P and SPC/E) associated with FFs.[69,74] From the non-polarizable FFs, the ff15ipq FF coupled with the SPC/E_b water model shows the best prediction of the relaxation parameters. This is in agreement with a recent study[75] and highlights the fact that it has been explicitly optimized to mimic the rotational diffusion of proteins.[29] As can be seen on Figure 3 and Table 3, the prediction of relaxation terms is significantly different from what is predicted with the use of the experimental D_{rot}, except for the AMOEBA FF and to a lesser extent for ff99SB-disp. For these FFs, the shape of the relaxation parameters values plotted along the UIM sequence experiences a slight shift compared to the relaxation parameters values when the experimental D_{iso} is included in the analysis. The most striking difference occurs for the ff15ipq and C36m FFs where residues located in the α-helix region have a marked decrease in R_2 and increase in R_1 compared to their values predicted with the experimental D_{iso} and D_{Δ}. This observation directly recalls that the rotational anisotropy is a major component of the relaxation

parameters and also reflects the orientation of NH bond vectors with respect to the rotational diffusion tensor. This orientation will align the NH vectors in the α-helix along the axis of fast overall rotation (see Figure S2). As a result, they will experience slower rates of overall tumbling (hence higher R_2s) compared to the rest of the protein, as it has been demonstrated in Figure 1. In the case of ff15ipq or C36m, the situation is contrasted with a significant contribution of $D_\perp$ that represent the axis of slower overall rotation (see Table 3). For these FFs, NH vectors will be affected more drastically by $D_\perp$ and will experience faster rates of overall tumbling (hence a decrease of their R_2s).

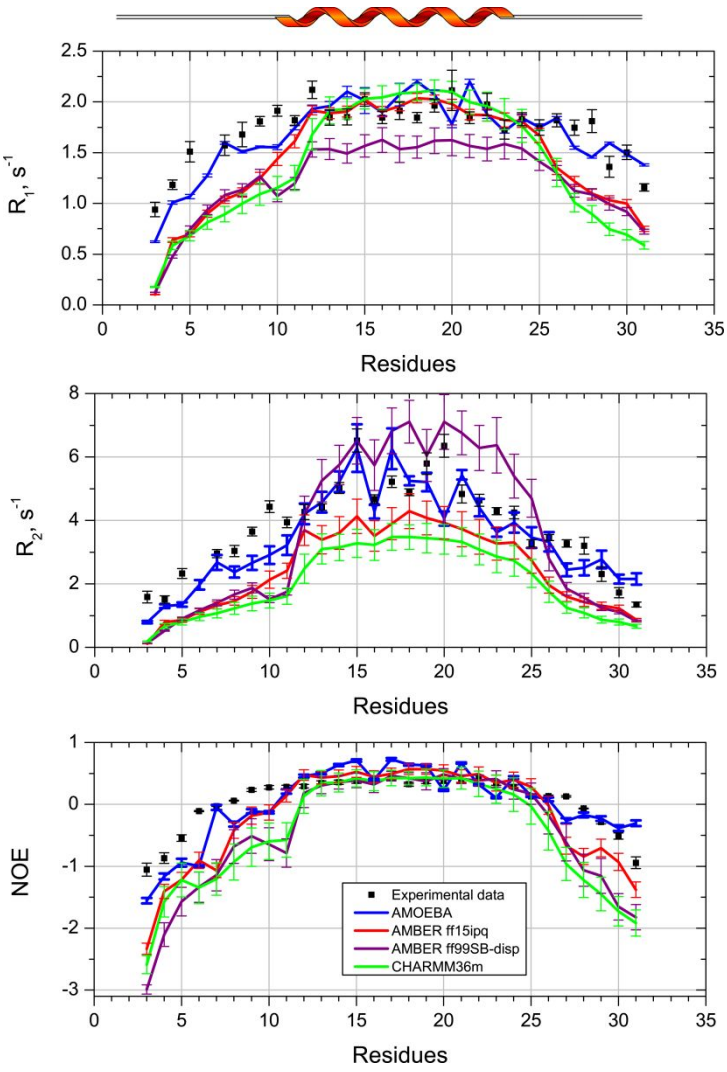

Figure 3. Experimental (black symbols) and computed NMR spin relaxation parameters (lines) R_1, R_2 and NOE for the different FFs used in this study. The global rotational diffusion D_{iso} is determined by MD while the zero order correction parameter ζ has been fixed to 0.89.[72] The UIM secondary structure is sketched at the top of the relaxation parameters.

On the other hand, the ff99SB-disp and AMOEBA FFs have a comparable contribution to $D_{\perp}$ compared to the experimental one. As a consequence, the values of the relaxation parameters for the residues in the α-helix region are less affected when the experimental D_{iso} is used (Figure 3). For the residues in the flexible regions, practically no difference could be noticed. This is likely due to the orientation of NH vectors which coordinates combine components on $D_{||}$ and $D_{\perp}$ and differ from the orientation of the NH vectors located in the α-helix. Thus, they are less sensitive to any change of the components of the diffusion tensor, as can be seen on the simulated relaxation parameters (see Figure S1B lower row). This observation has been made also in the past and revealed that a marked anisotropy combined with different orientation of the NH vectors may lead to important deviation of the transverse relaxation rates.[47]

CONCLUSION

Our results clearly indicate that the introduction of polarizable effects improve not only the modeling of fast local motion but also the global molecular reorientation delineated by its rotational diffusion tensor D_{rot} in case of a significant rotational anisotropy. Moreover,

an excellent prediction of the relaxation parameters has been reached without any requirement to a scaling factor used to compensate the prediction of the rotational diffusion. Overall, several conclusions may be drawn from our calculations: i) While polarization is highly anisotropic in water, the polarizable AMOEBA FF quantitatively predicts D_{iso} and D_{Δ} or their components $D_{||}$ and $D_{\perp}$. ii) The AMOEBA FF allows the accurate prediction of the ^{15}N R_1, ^{15}N R_2 and heteronuclear ^{1}H-^{15}N NOE relaxation parameters not only in well-structured but also in more flexible regions. This being said, we have shown that the use of the polarizable AMOEBA FF presents a convincing alternative to non-polarizable FFs when dealing with a mix of well-structured and flexible parts. Although its high computational cost with respect to conventional FFs, we are convinced that the next generation of hardware development will furnish sufficient computational power to alleviate the problem of computational time. We think that the use of polarizable FF will improve our understanding of protein dynamics especially in the case of IDPs, multidomain proteins or in crowded environment where charge distributions or protein shape are constantly remodeled over time.

ASSOCIATED CONTENT

Supporting Information. Details regarding structure of UIM domain, rotational diffusion analysis, radius of gyration, correlation function analysis and figures S1, S2, S3, S4 and S5 (PDF).

AUTHOR INFORMATION

Corresponding Author

*olivier.walker@univ-lyon1.fr

Author Contributions

The manuscript was written through contributions of all authors. All authors have given approval to the final version of the manuscript.

Notes

The authors declare no competing financial interests.

ACKNOWLEDGMENT

The current study was supported by a grant overseen by the French National Research Agency (ANR) as part of the “OH risque” programme (Metadyn, ANR-14-OHRI-0006-01). This work was performed using HPC resources from GENCI-CINES (Grant 2019-A0060707607). We thank the Rovaltain Foundation and ICL for providing experimental NMR time. We are grateful to Dr. Paul Robustelli for providing us the Amber ff99SB-disp formatted for use in Gromacs, Prof. Odile Eisenstein for useful discussion regarding polarizable force fields and Dr. Po-Chia Chen for fruitful discussion regarding SpinRelax.

ABBREVIATIONS

STAM2 (Signal Transducing Adaptator Molecule 2), UIM (Ubiquitin Interacting Motif), AMOEBA (Atomic Multipole Optimized Energetics for Biomolecular Application)

REFERENCES

1. Davis, D. G.; Perlman, M. E.; London, R. E., Direct Measurements of the Dissociation-Rate Constant for Inhibitor-Enzyme Complexes Via the T1ρ and T2 (CPMG) Methods. *J Magn Reson B* **1994,** *104* (3), 266-275.

2. Peng, J. W., Exposing the Moving Parts of Proteins with NMR Spectroscopy. *J Phys Chem Lett* **2012,** *3* (8), 1039-1051.

3. Palmer, A. G., NMR Characterization of the Dynamics of Biomacromolecules. *Chem Rev* **2004,** *104* (8), 3623-3640.

4. Abragam, P. A.; Abragam, A., *The Principles of Nuclear Magnetism*. Clarendon Press: 1961.

5. Peng, J. W.; Wagner, G., Mapping of the Spectral Densities of N-H Bond Motions in Eglin C Using Heteronuclear Relaxation Experiments. *Biochemistry* **1992,** *31* (36), 8571-8586.

6. Peng, J. W.; Wagner, G., Mapping of Spectral Density Functions Using Heteronuclear NMR Relaxation Measurements. *J Magn Reson* **1992,** *98* (2), 308-332.

7. Farrow, N. A.; Zhang, O.; Szabo, A.; Torchia, D. A.; Kay, L. E., Spectral Density Function Mapping Using 15N Relaxation Data Exclusively. *J Biomol NMR* **1995,** *6* (2), 153-162.

8. Ishima, R.; Nagayama, K., Protein Backbone Dynamics Revealed by Quasi Spectral Density Function Analysis of Amide N-15 Nuclei. *Biochemistry* **1995,** *34* (10), 3162-3171.

9. Lipari, G.; Szabo, A., Model-Free Approach to the Interpretation of Nuclear Magnetic Resonance Relaxation in Macromolecules. 1. Theory and Range of Validity. *J Am Chem Soc* **1982,** *104* (17), 4546-4559.

10. Lipari, G.; Szabo, A., Model-Free Approach to the Interpretation of Nuclear Magnetic Resonance Relaxation in Macromolecules. 2. Analysis of Experimental Results. *J Am Chem Soc* **1982,** *104* (17), 4559-4570.

11. Halle, B.; Wennerström, H., Interpretation of Magnetic Resonance Data from Water Nuclei in Heterogeneous Systems. *J Chem Phys* **1981,** *75* (4), 1928-1943.

12. Tchaicheeyan, O.; Mendelman, N.; Zerbetto, M.; Meirovitch, E., Local Ordering at Mobile Sites in Proteins: Combining Perspectives from NMR Relaxation and Molecular Dynamics. *J Phys Chem B* **2019,** *123* (13), 2745-2755.

13. Giupponi, G.; Harvey, M. J.; De Fabritiis, G., The Impact of Accelerator Processors for High-Throughput Molecular Modeling and Simulation. *Drug Discov Today* **2008,** *13* (23–24), 1052-1058.

14. Showalter, S. A.; Brüschweiler, R., Validation of Molecular Dynamics Simulations of Biomolecules Using NMR Spin Relaxation as Benchmarks: Application to the Amber99sb Force Field. *J. Chem. Theory Comput* **2007,** *3* (3), 961-975.

15. Chen, P. C.; Hologne, M.; Walker, O.; Hennig, J., Ab Initio Prediction of NMR Spin Relaxation Parameters from Molecular Dynamics Simulations. *J. Chem. Theory Comput* **2018,** *14* (2), 1009-1019.

16. Anderson, J. S.; Hernández, G.; LeMaster, D. M., Prediction of Bond Vector Autocorrelation Functions from Larmor Frequency-Selective Order Parameter Analysis of NMR Relaxation Data. *J. Chem. Theory Comput* **2017,** *13* (7), 3276-3289.

17. Prompers, J. J.; Br¬∏schweiler, R., General Framework for Studying the Dynamics of Folded and Nonfolded Proteins by NMR Relaxation Spectroscopy and MD Simulation. *J Am Chem Soc* **2002,** *124* (16), 4522-4534.

18. Hoffmann, F.; Xue, M.; Schäfer, L. V.; Mulder, F. A. A., Narrowing the Gap between Experimental and Computational Determination of Methyl Group Dynamics in Proteins. *Phys Chem Chem Phys* **2018,** *20* (38), 24577-24590.

19. Hoffmann, F.; Mulder, F. A. A.; Schäfer, L. V., Accurate Methyl Group Dynamics in Protein Simulations with Amber Force Fields. *J Phys Chem B* **2018,** *122* (19), 5038-5048.

20. Chen, P. C.; Hologne, M.; Walker, O., Computing the Rotational Diffusion of Biomolecules Via Molecular Dynamics Simulation and Quaternion Orientations. *J Phys Chem B* **2017,** *121* (8), 1812-1823.

21. Ollila, O. H. S.; Heikkinen, H. A.; Iwaï, H., Rotational Dynamics of Proteins from Spin Relaxation Times and Molecular Dynamics Simulations. *J Phys Chem B* **2018,** *122* (25), 6559-6569.

22. Polimeno, A.; Zerbetto, M., Evaluating Rotation Diffusion Properties of Molecules from Short Trajectories. *Phys Chem Chem Phys* **2019,** *21* (7), 3662-3668.

23. Kämpf, K.; Izmailov, S. A.; Rabdano, S. O.; Groves, A. T.; Podkorytov, I. S.; Skrynnikov, N. R., What Drives 15N Spin Relaxation in Disordered Proteins? Combined NMR/MD Study of the H4 Histone Tail. *Biophys J* **2018,** *115* (12), 2348-2367.

24. Salvi, N.; Abyzov, A.; Blackledge, M., Solvent-Dependent Segmental Dynamics in Intrinsically Disordered Proteins. *Sci Adv* **2019,** *5* (6), eaax2348.

25. Hall, J. B.; Fushman, D., Characterization of the Overall and Local Dynamics of a Protein with Intermediate Rotational Anisotropy: Differentiating between Conformational Exchange and Anisotropic Diffusion in the B3 Domain of Protein G. *J Biomol NMR* **2003,** *27* (3), 261-75.

26. Smith, P. E.; van Gunsteren, W. F., Translational and Rotational Diffusion of Proteins. *J Mol Biol* **1994,** *236* (2), 629-636.

27. Wong, K.-B.; Daggett, V., Barstar Has a Highly Dynamic Hydrophobic Core: Evidence from Molecular Dynamics Simulations and Nuclear Magnetic Resonance Relaxation Data. *Biochemistry* **1998,** *37* (32), 11182-11192.

28. Anderson, J. S.; LeMaster, D. M., Rotational Velocity Rescaling of Molecular Dynamics Trajectories for Direct Prediction of Protein NMR Relaxation. *Biophys Chem* **2012,** *168-169*, 28-39.

29. Takemura, K.; Kitao, A., Water Model Tuning for Improved Reproduction of Rotational Diffusion and NMR Spectral Density. *J Phys Chem B* **2012,** *116* (22), 6279-6287.

30. Robustelli, P.; Trbovic, N.; Friesner, R. A.; Palmer, A. G., Conformational Dynamics of the Partially Disordered Yeast Transcription Factor Gcn4. *J. Chem. Theory Comput* **2013,** *9* (11), 5190-5200.

31. Dauber-Osguthorpe, P.; Hagler, A. T., Biomolecular Force Fields: Where Have We Been, Where Are We Now, Where Do We Need to Go and How Do We Get There? *J Comput Aided Mol Des* **2019,** *33* (2), 133-203.

32. Nerenberg, P. S.; Head-Gordon, T., New Developments in Force Fields for Biomolecular Simulations. *Curr Opin Struct Biol* **2018,** *49*, 129-138.

33. Zhang, H.; Yin, C.; Jiang, Y.; van der Spoel, D., Force Field Benchmark of Amino Acids: I. Hydration and Diffusion in Different Water Models. *J Chem Inf Model* **2018,** *58* (5), 1037-1052.

34. Lemkul, J. A.; Huang, J.; Roux, B.; MacKerell, A. D., An Empirical Polarizable Force Field Based on the Classical Drude Oscillator Model: Development History and Recent Applications. *Chem Rev* **2016,** *116* (9), 4983-5013.

35. Shi, Y.; Xia, Z.; Zhang, J.; Best, R.; Wu, C.; Ponder, J. W.; Ren, P., Polarizable Atomic Multipole-Based Amoeba Force Field for Proteins. *J. Chem. Theory Comput* **2013,** *9* (9), 4046-4063.

36. Jing, Z.; Liu, C.; Cheng, S. Y.; Qi, R.; Walker, B. D.; Piquemal, J.-P.; Ren, P., Polarizable Force Fields for Biomolecular Simulations: Recent Advances and Applications. *Annu Rev Biophys* **2019,** *48* (1), 371-394.

37. Ouyang, J. F.; Bettens, R. P. A., When Are Many-Body Effects Significant? *J. Chem. Theory Comput* **2016,** *12* (12), 5860-5867.

38. Lin, Z.; van Gunsteren, W. F., Effects of Polarizable Solvent Models Upon the Relative Stability of an α-Helical and a β-Hairpin Structure of an Alanine Decapeptide. *J. Chem. Theory Comput* **2015,** *11* (5), 1983-1986.

39. Robustelli, P.; Piana, S.; Shaw, D. E., Developing a Molecular Dynamics Force Field for Both Folded and Disordered Protein States. *Proc Natl Acad Sci U S A* **2018,** *115* (21), E4758-E4766.

40. Debiec, K. T.; Cerutti, D. S.; Baker, L. R.; Gronenborn, A. M.; Case, D. A.; Chong, L. T., Further Along the Road Less Traveled: Amber Ff15ipq, an Original Protein Force Field Built on a Self-Consistent Physical Model. *J. Chem. Theory Comput* **2016,** *12* (8), 3926-3947.

41. Huang, J.; Rauscher, S.; Nawrocki, G.; Ran, T.; Feig, M.; de Groot, B. L.; Grubmuller, H.; MacKerell, A. D., Jr., Charmm36m: An Improved Force Field for Folded and Intrinsically Disordered Proteins. *Nat Methods* **2017,** *14* (1), 71-73.

42. Fushman, D.; Cahill, S.; Cowburn, D., The Main-Chain Dynamics of the Dynamin Pleckstrin Homology (Ph) Domain in Solution: Analysis of 15N Relaxation with Monomer/Dimer Equilibration. *J Mol Biol* **1997,** *266* (1), 173-94.

43. Ghose, R.; Fushman, D.; Cowburn, D., Determination of the Rotational Diffusion Tensor of Macromolecules in Solution from NMR Relaxation Data with a Combination of Exact and Approximate Methods--Application to the Determination of Interdomain Orientation in Multidomain Proteins. *J Magn Reson* **2001,** *149* (2), 204-217.

44. Mueller, L. J., Tensors and Rotations in NMR. *Concept Magn Reson A* **2011,** *38A* (5), 221-235.

45. Tjandra, N.; Feller, S. E.; Pastor, R. W.; Bax, A., Rotational Diffusion Anisotropy of Human Ubiquitin from 15N NMR Relaxation. *J Am Chem Soc* **1995,** *117* (50), 12562-12566.

46. Lee, L. K.; Rance, M.; Chazin, W. J.; Palmer, A. G., Rotational Diffusion Anisotropy of Proteins from Simultaneous Analysis of 15N and 13Cα Nuclear Spin Relaxation. *J Biomol NMR* **1997,** *9* (3), 287-298.

47. Fushman, D.; Cowburn, D., Characterization of Inter-Domain Orientations in Solution Using the NMR Relaxation Approach. In *Protein NMR for the Millennium*, Krishna, N. R.; Berliner, L. J., Eds. Springer: 2002; pp 53-77.

48. Fushman, D.; Xu, R.; Cowburn, D., Direct Determination of Changes of Interdomain Orientation on Ligation: Use of the Orientational Dependence of 15N NMR Relaxation in Abl Sh(32). *Biochemistry* **1999,** *38* (32), 10225-30.

49. Lange, A.; Castañeda, C.; Hoeller, D.; Lancelin, J.-M.; Fushman, D.; Walker, O., Evidence for Cooperative and Domain-Specific Binding of the Signal Transducing Adaptor Molecule 2 (Stam2) to Lys63-Linked Diubiquitin. *J Biol Chem* **2012,** *287* (22), 18687-18699.

50. Swanson, K. A.; Kang, R. S.; Stamenova, S. D.; Hicke, L.; Radhakrishnan, I., Solution Structure of Vps27 Uim-Ubiquitin Complex Important for Endosomal Sorting and Receptor Downregulation. *EMBO J* **2003,** *22* (18), 4597-4606.

51. Sali, A.; Blundell, T. L., Comparative Protein Modelling by Satisfaction of Spatial Restraints. *J Mol Biol* **1993,** *234* (3), 779-815.

52. Berendsen, H. J. C.; van der Spoel, D.; van Drunen, R., Gromacs: A Message-Passing Parallel Molecular Dynamics Implementation. *Comput Phys Commun* **1995,** *91* (1), 43-56.

53. Harvey, M. J.; Giupponi, G.; Fabritiis, G. D., Acemd: Accelerating Biomolecular Dynamics in the Microsecond Time Scale. *J. Chem. Theory Comput* **2009,** *5* (6), 1632-1639.

54. Eastman, P.; Swails, J.; Chodera, J. D.; McGibbon, R. T.; Zhao, Y.; Beauchamp, K. A.; Wang, L.-P.; Simmonett, A. C.; Harrigan, M. P.; Stern, C. D.; et al., Openmm 7: Rapid Development of High Performance Algorithms for Molecular Dynamics. *PLoS Comput Biol* **2017,** *13* (7), e1005659.

55. Harger, M.; Li, D.; Wang, Z.; Dalby, K.; Lagardère, L.; Piquemal, J.-P.; Ponder, J.; Ren, P., Tinker-Openmm: Absolute and Relative Alchemical Free Energies Using Amoeba on Gpus. *J Comput Chem* **2017,** *38* (23), 2047-2055.

56. Bussi, G.; Donadio, D.; Parrinello, M., Canonical Sampling through Velocity Rescaling. *J Chem Phys* **2007,** *126* (1), 014101-014101.

57. Berendsen, H. J. C.; Postma, J. P. M.; van Gunsteren, W. F.; DiNola, A.; Haak, J. R., Molecular Dynamics with Coupling to an External Bath. *J Chem Phys* **1984,** *81* (8), 3684-3690.

58. Essmann, U.; Perera, L.; Berkowitz, M. L.; Darden, T.; Lee, H.; Pedersen, L. G., A Smooth Particle Mesh Ewald Method. *J Chem Phys* **1995,** *103* (19), 8577-8593.

59. Hess, B., P-Lincs: A Parallel Linear Constraint Solver for Molecular Simulation. *J. Chem. Theory Comput* **2008,** *4* (1), 116-122.

60. Miyamoto, S.; Kollman, P. A., Settle: An Analytical Version of the Shake and Rattle Algorithm for Rigid Water Models. *J Comput Chem* **1992,** *13* (8), 952-962.

61. Friedrichs, M. S.; Eastman, P.; Vaidyanathan, V.; Houston, M.; Legrand, S.; Beberg, A. L.; Ensign, D. L.; Bruns, C. M.; Pande, V. S., Accelerating Molecular Dynamic Simulation on Graphics Processing Units. *J Comput Chem* **2009,** *30* (6), 864-872.

62. Zhang, C.; Lu, C.; Jing, Z.; Wu, C.; Piquemal, J.-P.; Ponder, J. W.; Ren, P., Amoeba Polarizable Atomic Multipole Force Field for Nucleic Acids. *J. Chem. Theory Comput* **2018,** *14* (4), 2084-2108.

63. Simmonett, A. C.; Pickard, F. C. t.; Ponder, J. W.; Brooks, B. R., An Empirical Extrapolation Scheme for Efficient Treatment of Induced Dipoles. *J Chem Phys* **2016,** *145* (16), 164101-164101.

64. Woessner, D. E., Nuclear Spin Relaxation in Ellipsoids Undergoing Rotational Brownian Motion. *J Chem Phys* **1962,** *37* (3), 647-654.

65. Lange, A.; Castaneda, C.; Hoeller, D.; Lancelin, J.-M.; Fushman, D.; Walker, O., Evidence for Cooperative and Domain-Specific Binding of the Signal Transducing Adaptor Molecule 2 (Stam2) to Lys(63)-Linked Diubiquitin. *J Biol Chem* **2012,** *287* (22), 18687-18699.

66. Walker, O.; Varadan, R.; Fushman, D., Efficient and Accurate Determination of the Overall Rotational Diffusion Tensor of a Molecule from 15N Relaxation Data Using Computer Program Rotdif. *J Magn Reson* **2004,** *168* (2), 336-345.

67. Berlin, K.; Longhini, A.; Dayie, T. K.; Fushman, D., Deriving Quantitative Dynamics Information for Proteins and Rnas Using Rotdif with a Graphical User Interface. *J Biomol NMR* **2013,** *57* (4), 333-52.

68. Knapp, B.; Ospina, L.; Deane, C. M., Avoiding False Positive Conclusions in Molecular Simulation: The Importance of Replicas. *J. Chem. Theory Comput* **2018,** *14* (12), 6127-6138.

69. Wong, V.; Case, D. A., Evaluating Rotational Diffusion from Protein MD Simulations. *J Phys Chem B* **2008,** *112* (19), 6013-6024.

70. Linke, M.; Köfinger, J.; Hummer, G., Rotational Diffusion Depends on Box Size in Molecular Dynamics Simulations. *J Phys Chem Lett* **2018,** *9* (11), 2874-2878.

71. Yeh, I.-C.; Hummer, G., System-Size Dependence of Diffusion Coefficients and Viscosities from Molecular Dynamics Simulations with Periodic Boundary Conditions. *J Phys Chem B* **2004,** *108* (40), 15873-15879.

72. Case, D. A., Calculations of NMR Dipolar Coupling Strengths in Model Peptides. *J Biomol NMR* **1999,** *15* (2), 95-102.

73. Fushman, D.; Varadan, R.; Assfalg, M.; Walker, O., Determining Domain Orientation in Macromolecules by Using Spin-Relaxation and Residual Dipolar Coupling Measurements. *Prog Nucl Magn Reson Spectrosc* **2004,** *44* (3-4), 189-214.

74. González, M. A.; Abascal, J. L. F., The Shear Viscosity of Rigid Water Models. *J Chem Phys* **2010,** *132* (9), 096101.

75. Zapletal, V.; Mládek, A.; Melková, K.; Louša, P.; Nomilner, E.; Jaseňáková, Z.; Kubáň, V.; Makovická, M.; Laníková, A.; et al., Choice of Force Field for Proteins Containing Structured and Intrinsically Disordered Regions. *Biophys J* **2020,** *118* (7), 1621-1633.

TOC Graphic.